

Motion Determination in Actin Filament Fluorescence Images with a Spatio-Temporal Orientation Analysis Method

Dietmar Uttenweiler,^{*†} Claudia Veigel,^{*‡} Rosemarie Steubing,^{*} Carlo Götz,^{*†} Sven Mann,^{*†} Horst Haussecker,[†] Bernd Jähne,[†] and Rainer H. A. Fink^{*}

^{*}Institut für Physiologie und Pathophysiologie, and [†]Interdisziplinäres Zentrum für wissenschaftliches Rechnen, Ruprecht-Karls-Universität Heidelberg, 69120 Heidelberg, Germany and [‡]Department of Biology, University of York, York YO10 5DD, United Kingdom

ABSTRACT We present a novel approach of automatically measuring motion in series of microscopic fluorescence images. As a differential method, the three-dimensional structure tensor technique is used to calculate the displacement vector field for every image of the sequence, from which the velocities are subsequently derived. We have used this method for the analysis of the movement of single actin filaments in the *in vitro* motility assay, where fluorescently labeled actin filaments move over a myosin decorated surface. With its fast implementation and subpixel accuracy, this approach is, in general, very valuable for analyzing dynamic processes by image sequence analysis.

INTRODUCTION

Fluorescence imaging techniques have emerged to be of central importance in the study of cellular and its underlying molecular function. Especially the possibility of monitoring processes with high spatial and temporal resolution makes this technique a unique tool for analyzing dynamic cellular and molecular processes (Uttenweiler and Fink, 1999). However, the automated quantitative determination of motion in sequences of images is one of the most challenging applications of modern image processing yet to be fully established. In particular, this applies for fast, temporally resolved images of single-molecule fluorescence with generally low signal-to-noise (S/N) ratio. The *in vitro* motility assay originally devised by Kron and Spudich (1986) is a typical example, where very high demands are posed on automated algorithms used for the quantification of motion. In this assay, fluorescently labeled actin filaments move over a surface of immobilized myosin or heavy meromyosin. Many parameters of this motion have been shown to be of significant importance for our understanding of the actomyosin interaction, e.g., the filament velocity is thought to be highly correlated to the unloaded shortening velocity of muscle fibers (for a more detailed discussion see Canepari et al., 1999) and therefore a direct reflection of the cross-bridge turnover rate (Cuda et al., 1997). Also, this assay is ideally suited to screen the functional domains of myosin, such as the nucleotide binding site, the actin binding site, the converter region and the lever arm (Sweeney et al., 1998; Kurzawa-Goertz et al., 1998; Murphy and Spudich, 1998; Uyeda et al., 1994, 1996; Holmes, 1996, 1997).

Furthermore myosin isoforms (Umemoto and Sellers, 1990; Harris et al., 1994) and actin mutants as e.g., described in Anson et al. (1995) can be selectively studied in this assay. Therefore, an accurate and standardized determination of the various parameters of actin filament motion is of vital importance for exploiting the full power of this assay.

Current techniques for automated determination of motion in series of images are mostly based on particle tracking algorithms with a preceding segmentation (Marston et al., 1996; Sellers et al., 1993; Work and Warshaw, 1992). Segmentation in low light level images with a low S/N ratio is still a process, which is subject to arbitrary and selective assumptions. Furthermore, particle tracking algorithms inherently suffer from major problems, as e.g., described in Fig. 1. For determining the actin filament motion in the *in vitro* motility assay, these algorithms mostly use the centroid of the filaments to calculate their displacement and hence their velocity. As pointed out by several groups (Hamelink et al., 1999a,b; Uttenweiler et al., 1999) this leads to an underestimation of actin filament speed when longer filaments are considered, which generally follow curved trajectories. The error depends on filament length and the curvature of the trajectory. Using only pointlike filaments is an arbitrary selection of filaments with the uncertainty of thereby selecting certain filament properties. Another problem of most automated algorithms is that nonmotile filaments are also assigned a nonzero velocity due to Brownian motion or jitter introduced by the acquisition hardware (Hamelink et al., 1999a,b; Gordon et al., 1997). This can lead to significant alterations in the histogram of filament velocities, i.e., introducing new apparent filament velocities, whose amplitudes are solely dependent on the fraction of nonmotile filaments and whose absolute values are strongly dependent on the frame rate of image acquisition (Hamelink et al., 1999a,b).

Also, many of these algorithms have not been tested on artificial data sets, which allow quantification of the accuracy of each method. Therefore, there is a large uncertainty if differences in filament velocities can be entirely ascribed

Received for publication 15 September 1999 and in final form 2 February 2000.

Address reprint requests to Dr. Dietmar Uttenweiler, Institut für Physiologie und Pathophysiologie, AG Medical Biophysics, Ruprecht-Karls-Universität Heidelberg, Im Neuenheimer Feld 326, 69120 Heidelberg, Germany. Tel.: +49-6221-544063; Fax: +49-6221-544123; E-mail: dietmar.uttweiler@urz.uni-heidelberg.de.

© 2000 by the Biophysical Society

0006-3495/00/05/2709/07 \$2.00

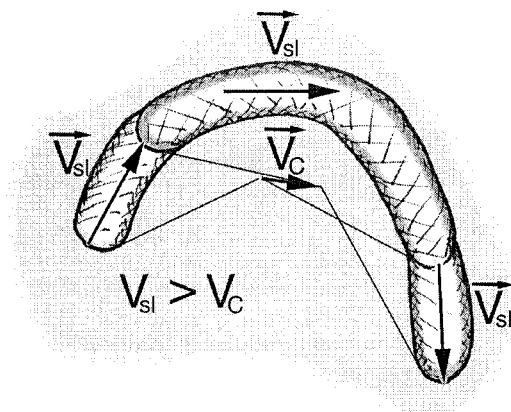


FIGURE 1 The centroid problem using common particle-tracking algorithms. If long filaments are analyzed with a particle-tracking algorithm, which uses the centroid for the velocity calculation, the tracking will reveal a velocity v_c , that is generally smaller than the actual sliding velocity v_{sl} .

to variations in the various parameters of the acto–myosin interaction, or to the different experimental conditions rather than to the different algorithms used for the analysis of the actin filament motion. Thus, it would be desirable to have an automated method for the measurement of actin filament speed, which reduces potential sources of error and allows specification of the accuracy of filament velocity determination.

Therefore, we have implemented an automated method using the structure tensor method for the determination of actin filament velocity in the *in vitro* motility assay with subpixel accuracy. To characterize the performance of the algorithm, we have tested the method on both artificial data sets and experimental data from rabbit fast skeletal myosin.

MATERIALS AND METHODS

In vitro motility assay

Protein isolation

Myosin was prepared basically according to Margossian and Lowey (1982) with some modifications according to Hynes et al. (1987). In brief, 20 g of rabbit skeletal muscle mince was extracted for 10 min at 4°C in 40 ml of 0.3 M KCl-buffer. The suspension was diluted twofold with cold water and centrifuged at 7000 rpm (Sorvall, rotor SA 600, 40-ml tubes). The ionic strength of the supernatant was lowered to 0.03 M, incubated 30 min in the cold and the precipitate was spun down at 7000 rpm for 10 min. The pellet was dissolved in 4 ml of 2.4 M KCl-buffer and actomyosin precipitated by adding cold H₂O very slowly, taking care not to lower the ionic strength below 0.3 M. Following centrifugation at 60,000 × *g* (Sorvall, rotor T-865, 30-ml Polycarbonate tubes) for 30 min, the myosin was precipitated by lowering the KCl-concentration to 0.03 M. Again, care was taken to add the water very slowly. The myosin was collected by centrifugation at 10,000 rpm (Sorvall, rotor GSA, 250-ml Polypropylene tubes) for 10 min and redissolved in a minimum volume of 3 M KCl-buffer. This [KCl] was lowered to ~1 M using 0.5 M KCl-buffer. A final centrifugation for 60 min at 160,000 × *g* (Sorvall, rotor T 1270, 10-ml Polycarbonate tubes) cleared

the myosin solution resulting in highly purified myosin with a yield of ~0.1%. From this pure myosin, heavy meromyosin (HMM) was prepared according to Kron et al. (1991).

Rabbit skeletal muscle actin was prepared according to Pardee and Spudich (1982) with minor modifications. Using collodion tubes reduced the dialysis time for depolymerization to one overnight dialysis, resulting in pure actin as indicated by SDS-PAGE.

Ten microliters of a 0.5-mg/ml dilution of F-actin in assay buffer (AB) (25 mM KCl, 4 mM MgCl₂, 1 mM EGTA, 25 mM imidazolium-chloride, pH = 7.5; Kron et al., 1991) was added to 90 μl 1.3 μM solution of tetramethylrhodamine-phalloidin (R-415, Molecular Probes, OR, USA) in AB buffer and incubated overnight on ice.

Preparation of flow cell

For the motility assay, a microscope flow cell was constructed from a precleaned 22 × 50 mm² glass microscope slide and a 22 × 40 mm² precleaned coverslip which was coated on one surface with 2 μl of 0.1% nitrocellulose dissolved in amyl acetate (Kron et al., 1991). Rabbit skeletal muscle HMM was allowed to bind to the nitrocellulose-coated coverslip by incubating 100 μl of 100 μg/ml HMM in the flow cell for 1 min. The coverslip surface was then blocked by allowing 100 μl of 0.5 mg/ml BSA in AB to flow into the flow cell and leaving for 2 min. 100 μl of rhodamine-phalloidin labeled actin filaments diluted in AB (1:100, v:v) were added to the flow cell. Following a washing step with 100 μl of 1 mg/ml BSA in AB, 100 μl of AB-GOC solution was added for visual microscopic detection of filament binding. AB-GOC was prepared as follows: AB was degassed with a vacuum pump, and then an oxygen scavenger system, to reduce photobleaching, of 20 mM DTT, 0.2 mg/ml glucose oxidase, 0.05 mg/ml catalase, and 3 mg/ml glucose was added, together with an ATP backup system (2 mM creatine phosphate, 0.1 mg/ml creatine phosphokinase). Actin filament movement was induced by exchanging the AB-GOC solution with an AB-GOC solution including 2 mM ATP. The experiments were carried out at 21°C.

Fluorescence imaging

The labeled filaments are observed through an inverted microscope (IX70, Olympus, Tokyo, Japan) equipped with epifluorescence (Xe-light source) and a 100× objective (UPLANFL, 1.3 NA, oil, Olympus, Tokyo, Japan) and visualized with an intensified CCD-Camera (Luminescence Imager, Photonic Science, Robertsbridge, UK) with fiber optical coupling. The image sequences are digitized with 8-bit resolution with a frame grabber (Meteor, Matrox, Dorval, Canada) and transferred to PC (Intel P200MMX, 96 MB main memory, WinNT 4.0) for analysis, storage and further evaluation. Additionally the sequences are also stored on video tape (AG-7355, Panasonic, Osaka, Japan).

Structure tensor method

The structure tensor method for a quantitative analysis of velocities in image sequences is a differential optical flow-based technique. The underlying idea is that motion in image sequences corresponds to oriented structures in the spatio-temporal *x*, *y*, *t*-domain (Haussecker and Spiess, 1999). This domain is spanned by the two image coordinates and augmented by the time as a third coordinate axis. Figure 2 shows how the displacement of an object within consecutive images results in inclined three-dimensional (3D) iso-grey-value structures in the spatio-temporal domain. The faster the object moves, the more inclined the structures get. For objects at rest, all iso-grey-value structures are oriented parallel to the temporal axis. From the orientation angle of the iso-grey-value lines in the

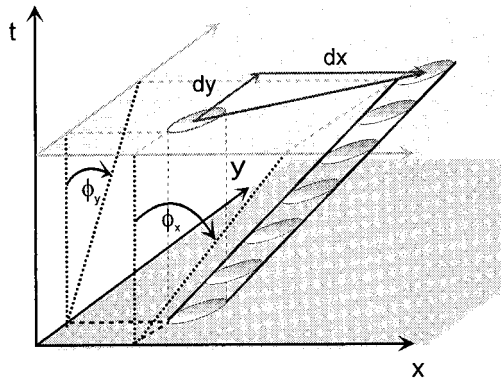


FIGURE 2 The displacement of structures in an image sequence corresponds to an orientation of iso-grey-values in the spatio-temporal x, y, t -domain. Therefore, the determination of displacements and, subsequently, velocities in an image sequence is equivalent to a 3D orientation analysis in the x, y, t -domain.

image sequence $g(x, y, t)$, the velocity \mathbf{u} can be calculated by

$$\mathbf{u} = - \begin{pmatrix} \tan \Phi_x \\ \tan \Phi_y \end{pmatrix}, \quad (1)$$

where the minus sign originates from the mathematical definition of a positive angle. Hence, motion analysis in image sequences is equivalent to an orientation analysis of the spatio-temporal image structure. To find the direction of iso-grey-value lines, we search the direction \mathbf{r} that is as much perpendicular as possible to all 3D gray-value gradients $\nabla g = [g_x, g_y, g_t]^T$ within a local neighborhood of the pixel of interest. In a least squares sense, the direction \mathbf{r} has to minimize the expression

$$S = \langle [\mathbf{r}^T (\nabla g)]^2 \rangle \rightarrow \min, \quad (2)$$

where $\langle \rangle$ denotes a local average of the expression within the brackets. Minimizing S with respect to the components $r_x, r_y,$ and r_t , we get the linear equation system,

$$\mathbf{J}\mathbf{r} = \lambda\mathbf{r}, \quad \text{with } J_{pq} = \langle g_p g_q \rangle, \quad (3)$$

where \mathbf{J} denotes the 3×3 symmetric structure tensor and λ the eigenvalue. With g_p and g_q , we denote the partial derivatives of g with respect to the p and q direction, respectively. Thus, the velocity determination leads to an eigenvalue-analysis of the structure tensor \mathbf{J} . The direction of minimal gray-value variation is given by the eigenvector of \mathbf{J} to the smallest eigenvalue.

The implementation of the structure tensor method can be carried out by standard image-processing operators, where each component of the structure tensor \mathbf{J} can be computed as

$$J_{pq} = B((D_p g) \cdot (D_q g)), \quad (4)$$

with a binomial filter B as a window function for local averaging and the first-order differential operators D_p and D_q in the p and q direction, respectively. After computing the components of \mathbf{J} , the eigenvalue analysis is carried out numerically using the Jacobi method. The angles Φ_x and Φ_y , and hence the velocity \mathbf{u} , can be computed from the projection of \mathbf{r} onto the $x-t$ and $y-t$ plane, respectively. Without going further into detail, we would like to point out an important feature of the structure tensor technique: In addition to the velocity \mathbf{u} , the technique yields normalized measures quantifying the precision of the estimate for every image point. This allows separation of reliable estimates from areas where no information can be

extracted and constitutes an important prerequisite for a statistical analysis of the motility assay. The detailed description of the structure tensor method for motion determination can be found in Haussecker and Spiess (1999).

The algorithms are implemented using the image-processing software Heurisko (AEON, Hanau, Germany). The spatial and temporal scaling of the velocity data is simply accomplished by multiplication of the corresponding scaling factors (micron/pixel and frames/s) with the displacements computed with the structure tensor method.

RESULTS

The method was first tested on computer-generated sequences to characterize its performance under known conditions. The displacement vectors and, subsequently, the velocity vectors determined by the structure tensor method are computed for every image of the image sequence. This can be done for the entire frame size or for smaller areas of interest (aoi) within the frame. From the velocity vectors, all other quantities, such as e.g., the absolute value of the velocity and hence the velocity distribution, can be derived. The test patterns used for the evaluation of the accuracy of the velocity determination is shown in the upper panels of Fig. 3. The objects are rodlike filaments with different lengths, which move in x - and y -direction, in a 45° degree angle and in an approximate circle, respectively. These motions represent a basis of possible displacements, from which all other movements can be derived. The displacement of objects in all sequences was 1 pixel/frame for the motion in x - y direction and for the approximate circular motion. The objects in the diagonal direction move with a displacement of $\sqrt{2}$ pixel/frame.

Figure 3 shows the results of velocity determinations with different levels of Gaussian noise superimposed on a test sequence of 100 frames. The images have 8-bit resolution (256 gray levels). The objects (rodlike filaments) are assigned a gray level of 200 versus the black background with a gray level of zero. The first sequence on the left panel contains no noise. Gaussian noise with a standard deviation of 30 gray values is added to the test sequence in the middle panel, and Gaussian noise with a standard deviation of 50 gray values is added to the sequence in the right panel.

The bin size of the velocity histograms for all test sequences was set to $1/30$ pixel/frame to quantify the subpixel accuracy of the method. All velocity histograms were subsequently fitted with a Gaussian distribution. The mean (μ) of the Gaussian distribution is taken as the measure of the peak velocity, and the broadness of the velocity distribution is characterized by twice the standard deviation (σ) of the Gaussian distribution.

The velocity histogram for the sequence with no noise in the left panel of Fig. 3 exhibits a very sharp peak centered at 1.00 pixel/frame with a broadness of 0.03 pixel/frame. The second peak is centered at 1.41 pixel/frame with a broadness of 0.03 pixel/frame. As can be seen in the middle panel of Fig. 3, the addition of noise leads to a broadening

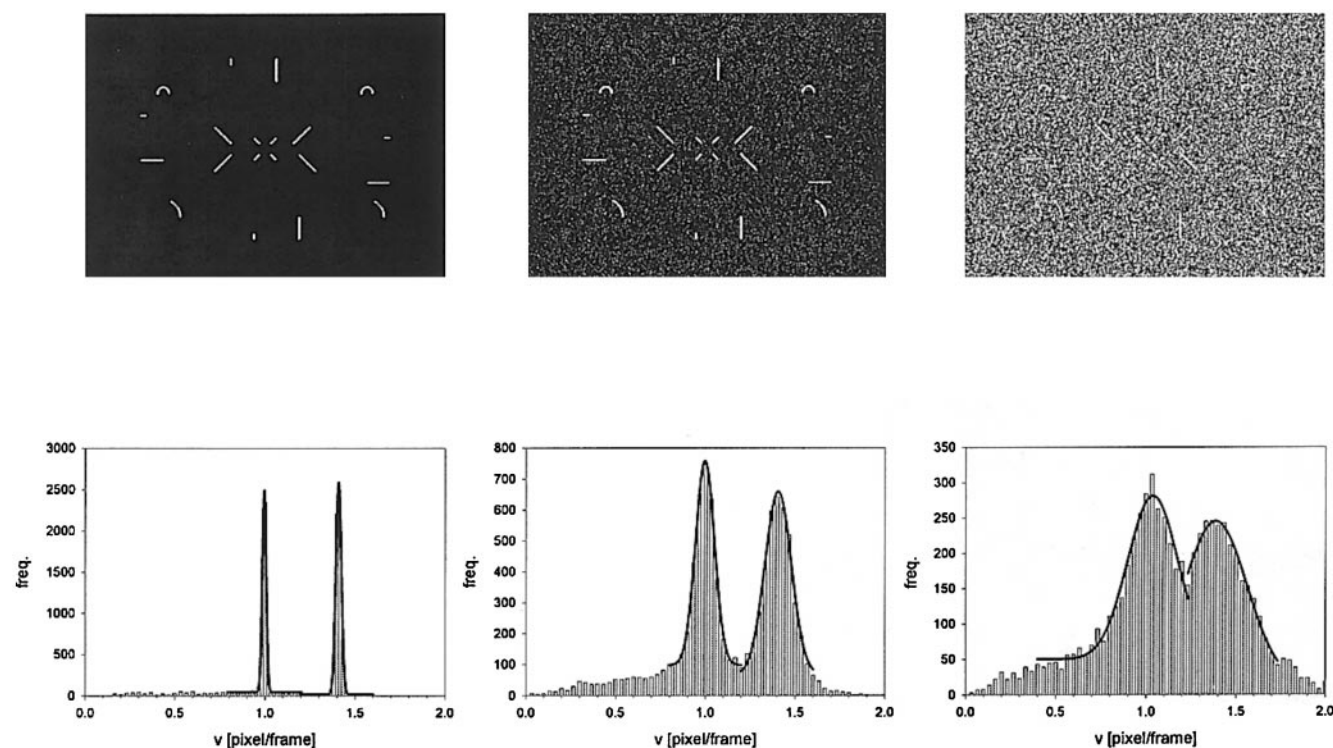


FIGURE 3 Test pattern used to analyze the accuracy of the velocity quantification. The rodlike objects (gray value 200) move in x , y direction, in a 45° degree angle and in approximated circles, respectively, versus a black background (gray value zero). The lower panels show the velocity distributions of the test patterns as obtained with the structure tensor method. The test pattern with no noise is shown on the left, the test pattern with added Gaussian noise with a standard deviation of 30 gray values is shown in the middle panel, and the test pattern with added Gaussian noise with a standard deviation of 50 gray values is shown in the right panel.

of the velocity histogram, but the center of the peak value is unbiased by the noise. The peaks are at 1.00 pixel/frame with a broadness of 0.11 pixel/frame and 1.41 pixel/frame with a broadness of 0.15 pixel/frame. With a very high amount of noise ($\sigma = 50$ gray values) applied in the right panel of Fig. 3, the first peak is centered at 1.04 pixel/frame with a broadness of 0.28 pixel/frame and the second peak is centered at 1.39 pixel/frame with a broadness of 0.35 pixel/frame.

These test sequences demonstrate the power of the structure tensor method to quantify velocities in sequences of noisy images without a bias in peak velocities. The resulting broadening of the distributions with higher amounts of Gaussian noise added to each pixel of the image series is correlated with the fact that the structure tensor is a pixel-based method. Test data with noninteger pixel/frame displacements were generated by recording the movement of fluorescent beads on the motorized stage of the inverted fluorescence microscope. None integer displacements/frame were not used in the computer generated test data, because of potential sources of errors introduced by the interpolation algorithms that have to be used to create such data. The accuracy of the method for these displacements is similar to that calculated with the artificial data (data not shown).

A comparison of the structure tensor method and a conventional tracking approach (Retrac 1.15 by Dr. Nick Carter, The Marie Curie Research Institute, Oxted, Surrey, U.K.) is shown in Fig. 4. Because of the centroid problem discussed in Fig. 1, we used a computer-assisted manual tracking system that does not use the centroid for the velocity determination, but uses the head and tail end of the filament to determine its velocity. Velocities determined from tracking heads and tails of the filaments were combined and averaged. The four circular movements of the test pattern shown in Fig. 3 with added Gaussian noise ($\sigma = 30$ gray values) were analyzed with both methods. Again, both velocity distributions were fitted with a Gaussian distribution. The tracking algorithm exhibits a generally broader velocity distribution and a 5% error in peak velocity ($v_{\max} = 1.05$ pixel/frame, $2\sigma = 0.39$ pixel/frame). In contrast, the structure tensor method is unbiased by the noise ($v_{\max} = 1.00$ pixel/frame) and exhibits a smaller broadness of the velocity distribution of 0.13 pixel/frame. It introduces some errors at small velocities ($v < 0.3$ pixel/frame), which originate from the fact that the displacements are calculated on the first level of a Gaussian pyramid to speed up the computations.

As an example of the application of the method to noisy fluorescence images, the analysis of the velocity distribu-

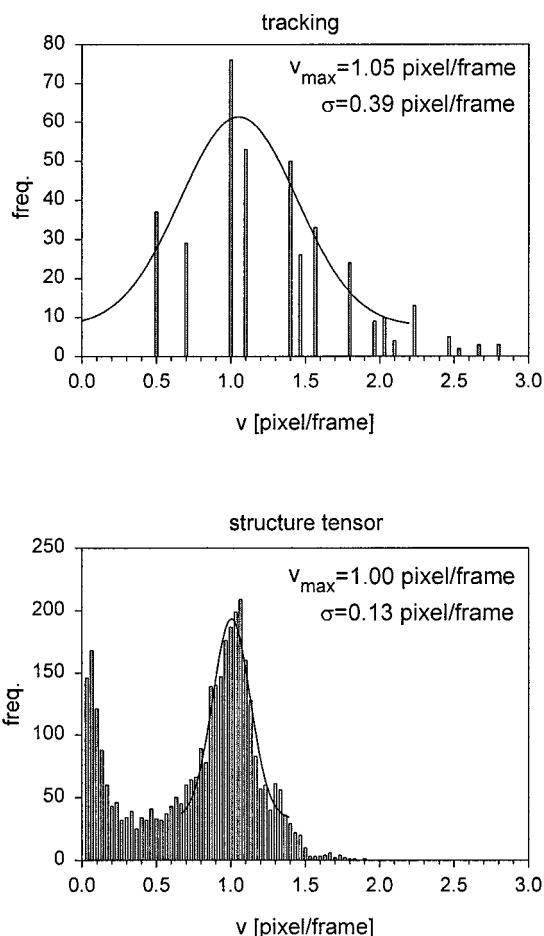


FIGURE 4 The four circular movements of the test pattern shown in Fig. 3 with added Gaussian noise ($\sigma = 30$ gray values) are analyzed with a conventional particle-tracking algorithm (*top*) and the structure tensor method (*bottom*). The particle-tracking method detects the peak velocity of 1 pixel/frame with an error of approximately 5% and the structure tensor method detects the peak velocity with an error of less than 1%. The tracking algorithm shows a significant scatter, which results in a very broad velocity distribution.

tion of actin filament movement in an *in vitro* motility experiment is shown in Fig. 5. Figure 5 *A* shows the four aoi selected for the analysis of the velocity distributions in the time series. Additionally, the velocity distribution for the entire frame is calculated. In Fig. 5 *B*, the resulting velocity histograms are plotted. One can distinguish different filament populations, a slow-moving population as analyzed in aoi1 with a filament speed of approximately $0.6 \mu\text{m/s}$ and a fast-moving population as analyzed in the other areas of interest with a mean speed of approximately $3 \mu\text{m/s}$ and a small fraction of filaments with velocities above $4 \mu\text{m/s}$ as detected in aoi3 and aoi4. The velocity distribution calculated for the entire frame has its peak velocity at $3.01 \mu\text{m/s}$ with a broadness of $0.67 \mu\text{m/s}$. The calculation is performed on the first level of a Gaussian pyramid and the time to calculate the velocity histogram for the entire frames of the

image sequence ($768 * 576$ pixel, 8 bit, 100 images) is less than one minute on a standard PC (see Materials and Methods). Figure 5 *B* additionally shows the velocity distribution as obtained with the previously described particle tracking algorithm. All motile filaments in the frame were tracked. After a filament stopped, it was discarded for the stop period. Again, the peak velocities as calculated by the structure tensor method ($v_{\max} = 3.01 \mu\text{m/s}$) and the particle tracking algorithm ($v_{\max} = 3.04 \mu\text{m/s}$) are very similar. The distribution obtained with the tracking algorithm is significantly broader ($2\sigma = 2.4 \mu\text{m/s}$) than the respective distribution obtained with the structure tensor method ($2\sigma = 1.34 \mu\text{m/s}$). This is in accordance with the results obtained with the test data described in Fig. 4, where the analysis of curved trajectories generally leads to a broader velocity distribution with the particle tracking algorithm. In most cases, curved trajectories are by far the most dominant movements of actin filaments in the *in vitro* motility assay.

DISCUSSION

The general importance of measuring motion in image sequences requires sophisticated concepts and algorithms to extract the motion parameters. In this work, we have presented a new approach of automatically calculating displacements, and hence velocities, in series of noisy fluorescence images with a pixel-based differential optical flow method. We have successfully applied it to the automated analysis of actin filament movement in the *in vitro* motility assay. Additionally, the method has been tested on computer-generated test sequences to characterize its performance under known conditions.

The main advantages of using this differential optical-flow-based technique can be summarized as follows: 1) The lack of segmentation before the velocity determination does not introduce any arbitrary and selective assumptions regarding object features. It also avoids the problem of segmentation problems in highly noisy fluorescence images. If object features are of interest, a segmentation can be accomplished by using the velocity field, avoiding the classical segmentation problems in noisy image data sets. 2) The structure tensor method is not biased by noise as are other techniques. As shown in Fig. 3, the superimposed noise leads to a broadening of the velocity distributions but does not result in a shift of the central velocity. As shown in Haussecker and Spiess (1999), this is a major problem when using other methods of velocity determination. 3) The method has a very high precision and determines the displacement vector field and hence the velocities with sub-pixel accuracy. 4) The velocity determination is independent of any arbitrary object features. 5) Features of the velocity field normally not accessible can be derived with this method as, e.g., the divergence of the velocity field in applications where motion is influenced by sink and sources

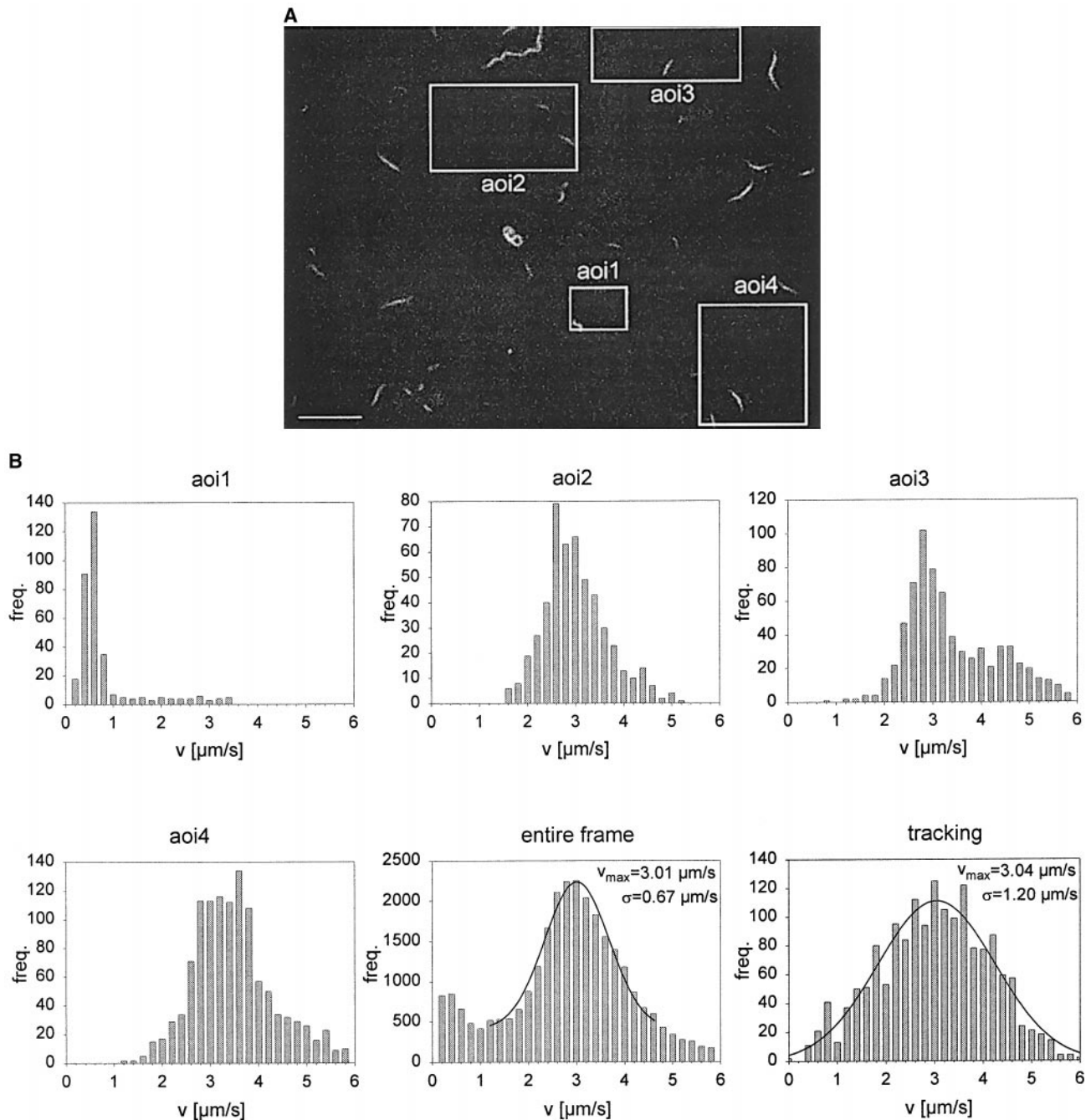


FIGURE 5 (A) Example of an analysis of 100 frames of motility assay data with the structure tensor method. For the analysis, aoi can be selected, where the displacement vector field and, subsequently, the velocity vector field are computed. Additionally, the entire frame can be analyzed. The scale bar is $10 \mu\text{m}$. (B) Histograms of velocity distributions in the areas of interests as shown in the previous panel. One can clearly see different populations of filaments (aoi1 $v_{\text{filament}} < 1 \mu\text{m/s}$, aoi3 two populations $v_{\text{filament1}} = 2.8 \mu\text{m/s}$ and $v_{\text{filament2}} = 4.5 \mu\text{m/s}$). The velocity histograms for the entire frame as obtained by the structure tensor method and with a conventional particle-tracking algorithm are shown in the middle lower and the right lower panel. As already indicated in Fig. 4, the tracking algorithm yields a much broader velocity distribution than the structure tensor method.

(e.g., in diffusion processes). 6) With its pyramidal implementation, the method is very fast and allows the calculation of the velocity vectors of series of images on standard PCs without the need of further sophisticated hardware. Furthermore, even dynamic processes that cannot be resolved as

single-particle motions, e.g., bulk diffusion processes, can now be analyzed within one theoretical and methodological framework.

We hope that this approach will be a substantial contribution to the general approaches of an automated and pre-

cise quantification of motion in the various applications of biophysical image sequence analysis.

Supported by grants from the Deutsche Forschungsgemeinschaft Fi 674/1–1 and Ja 395/6–2.

REFERENCES

- Anson, M., D. R. Drummond, M. A. Geeves, E. S. Hennessey, M. D. Ritchie, and J. C. Sparrow. 1995. Actomyosin kinetics and in vitro motility of wild-type *Drosophila* actin and the effects of two mutations in the Act88F gene. *Biophys. J.* 68:1991–2003.
- Canepari, M., R. Rossi, M. A. Pellegrino, C. Reggiani, and R. Bottinelli. 1999. Speeds of actin translocation in vitro by myosins extracted from single rat muscle fibers of different types. *Exp. Physiol.* 84:803–806.
- Cuda, G., E. Pate, R. Cooke, and J. R. Sellers. 1997. In vitro actin filament sliding velocities produced by mixtures of different types of myosin. *Biophys. J.* 72:1767–1779.
- Gordon, A. M., M. A. LaMadrid, Y. Chen, Z. Luo, and P. B. Chase. 1997. Calcium regulation of skeletal muscle thin filament in vitro. *Biophys. J.* 72:1295–1307.
- Hamelink, W., J. G. Zegers, B. W. Trijtel, and T. Blangé. 1999a. Path reconstruction method to determine actin filament speed in the in vitro motility assay. *J. Muscle Res. and Cell Motil.* 20:72 (Abstract).
- Hamelink, W., J. G. Zegers, B. W. Trijtel, and T. Blangé. 1999b. Path reconstruction as a tool for actin filament speed determination in the in vitro motility assay. *Anal. Biochem.* 273:12–19.
- Harris, D. E., S. S. Work, R. K. Wright, N. R. Alpert, and D. M. Warshaw. 1994. Smooth, cardiac and skeletal muscle myosin force and motion generation assessed by cross-bridge mechanical interactions in vitro. *J. Muscle Res. Cell. Motil.* 15:11–19.
- Haussecker, H., and H. Spiess. 1999. Motion. In *Handbook of Computer Vision and Applications*. B. Jähne, H. Haussecker, and P. Geissler, editors. Academic Press, San Diego. Vol. 2. 310–396.
- Holmes, K. C. 1996. Muscle proteins, their actions and interactions. *Curr. Opin. Struct. Biol.* 6:781–789.
- Holmes, K. C. 1997. The swinging lever arm hypothesis of muscle contraction. *Curr. Biol.* 7:R112–R118.
- Hynes, T. R., S. M. Block, B. T. White, and J. A. Spudich. 1987. Movement of myosin fragments in vitro: domains involved in force production. *Cell.* 48:953–963.
- Kron, S. J., and J. A. Spudich. 1986. Fluorescent actin filaments move on myosin fixed to a glass surface. *Proc. Natl. Acad. Sci. USA.* 83:6272–6276.
- Kron, S. J., Y. Y. Toyoshima, T. Q. P. Uyeda, and J. A. Spudich. 1991. Assays for actin sliding movement over myosin-coated surfaces. *Methods Enzymol.* 96:399–416.
- Kurzawa-Goertz, S. E., C. L. Perreault-Micale, K. M. Trybus, A. G. Szent-Gyorgyi, and M. A. Geeves. 1998. Loop I can modulate ADP affinity, ATPase activity, and motility of different scallop myosins. Transient kinetic analysis of S1 isoforms. *Biochemistry.* 37:7517–7525.
- Margossian, S. S., and S. Lowey. 1982. Preparation of myosin and its subfragments from rabbit skeletal muscle. *Methods Enzymol.* 85:55–71.
- Marston, S. B., I. D. C. Fraser, W. Bing, and G. Roper. 1996. A simple method for automated tracking of actin filaments in the motility assay. *J. Muscle Res. and Cell Motil.* 17:497–506.
- Murphy, C. T., and J. A. Spudich. 1998. Dictyostelium myosin 25–50K loop substitutions specifically affect ADP release rates. *Biochemistry.* 37:6738–6744.
- Pardee, J. D., and J. A. Spudich. 1982. Purification of muscle actin. *Methods Enzymol.* 85B:164–181.
- Sellers, J. R., G. Cuda, F. Wang, and E. Homsher. 1993. Myosin-specific adaptations of the motility assay. *Methods Cell Biol.* 39:23–49.
- Sweeney, H. L., S. S. Rosenfeld, F. Brown, L. Faust, J. Smith, J. Xing, L. A. Stein, and J. R. Sellers. 1998. Kinetic tuning of myosin via a flexible loop adjacent to the nucleotide binding pocket. *J. Biol. Chem.* 273:6262–6270.
- Umemoto, S., and J. R. Sellers. 1990. Characterization of in vitro motility assays using smooth muscle and cytoplasmic myosins. *J. Biol. Chem.* 265:14864–14869.
- Uttenweiler, D., and R. H. A. Fink. 1999. Dynamic fluorescence imaging. In *Handbook of Computer Vision and Applications*. B. Jähne, H. Haussecker, and P. Geissler, editors. Academic Press, San Diego. Vol. 1. 323–346.
- Uttenweiler, D., S. Mann, R. Steubing, C. Veigel, H. Haussecker, B. Jähne, and R. H. A. Fink. 1999. Actin filament sliding velocity in the motility assay analysed with the structure tensor method. *J. Muscle Res. and Cell Motil.* 20:74 (Abstract).
- Uyeda, T. Q., K. M. Ruppel, and J. A. Spudich. 1994. Enzymatic activities correlate with chimaeric substitutions at the actin-binding face of myosin. *Nature.* 368(6471):567–569.
- Uyeda, T. Q., P. D. Abramson, and J. A. Spudich. 1996. The neck region of the myosin motor domain acts as a lever arm to generate movement. *Proc. Natl. Acad. Sci. USA.* 93:4459–4464.
- Work, S. S., and D. M. Warshaw. 1992. Computer-assisted tracking of actin filament motility. *Analyt. Biochem.* 202:275–285.